Transient Nanoscopy of Exciton Dynamics in 2D Transition Metal Dichalcogenides

*Jingang Li, Rundi Yang, Naoki Higashitarumizu, Siyuan Dai, Junqiao Wu, Ali Javey, and Costas P. Grigoropoulos**

The electronic and optical properties of 2D transition metal dichalcogenides are dominated by strong excitonic resonances. Exciton dynamics plays a critical role in the functionality and performance of many miniaturized 2D optoelectronic devices; however, the measurement of nanoscale excitonic behaviors remains challenging. Here, a near-field transient nanoscopy is reported to probe exciton dynamics beyond the diffraction limit. Exciton recombination and exciton–exciton annihilation processes in monolayer and bilayer MoS_2 are studied as the proof-of-concept demonstration. Moreover, with the capability to access local sites, intriguing exciton dynamics near the monolayer-bilayer interface and at the MoS_2 nano-wrinkles are resolved. Such nanoscale resolution highlights the potential of this transient nanoscopy for fundamental investigation of exciton physics and further optimization of functional devices.

J. Li, R. Yang, C. P. Grigoropoulos
Laser Thermal Laboratory
Department of Mechanical Engineering
University of California
Berkeley, CA 94720, USA
E-mail: cgrigoro@berkeley.edu

N. Higashitarumizu, A. Javey
Department of Electrical Engineering and Computer Sciences
University of California
Berkeley, CA 94720, USA

N. Higashitarumizu, J. Wu, A. Javey
Materials Sciences Division
Lawrence Berkeley National Laboratory
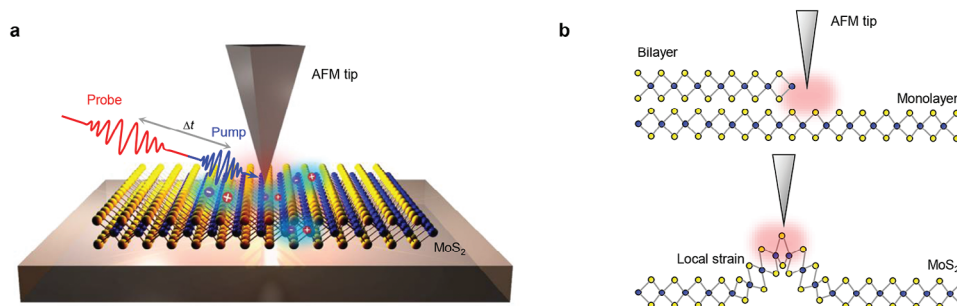Berkeley, CA 94720, USA

S. Dai
Materials Research and Education Center
Department of Mechanical Engineering
Auburn University
Auburn, AL 36849, USA

J. Wu
Department of Materials Science and Engineering
University of California
Berkeley, CA 94720, USA

1. Introduction

Atomically thin 2D transition metal dichalcogenides (TMDCs) exhibit many intriguing physical properties, including strong photoluminescence (PL) from monolayers, tunable bandgaps, and valley polarization.[1–3] The reduced dielectric screening and enhanced Coulomb interactions in TMDCs result in the formation of excitons (i.e., bound electron–hole pairs) at room temperature with much larger binding energies than those in conventional semiconductors.[4,5] The strong excitonic effects lead to pronounced light absorption and emission, making TMDCs promising for applications in photovoltaics, sensors, and light sources.[6–8] For instance, monolayer TMDCs have demonstrated superior performances in low-power transistors,[9] high-sensitivity photodetectors,[10] and low-threshold nanolasers.[11]

One of the most important aspects of 2D TMDC research is the dynamics of photoexcited excitons, which ultimately determine the efficiency of photonic and optoelectronic devices. The transient behaviors and relaxation pathways of excitons are of key significance for both fundamental study and technological innovation of TMDC materials.[12] Time-resolved PL (TRPL) spectroscopy has been widely utilized to measure the PL lifetime of monolayer TMDCs.[13] Alternatively, transient absorption (TA) spectroscopy traces the change in the absorption of single-layer or few-layer TMDCs to analyze the exciton recombination process.[14] Enhanced many-body interactions, such as Auger recombination and exciton–exciton annihilation (EEA), have been observed due to the reduced dimensionality.[15–17] As a nonradiative recombination process, EEA is found to be dominant at high excitation energy, which limits the device performance. With the integration of optical imaging techniques, TA microscopy has also been developed to investigate the transport and diffusion properties of excitons.[18–20] However, the spatial resolution of TRPL and TA is typically limited by optical diffraction, which prevents accessing the nanoscale heterogeneity of exciton dynamics.[21–23]

Scanning probe methods provide nanoscale spatial resolution to overcome the optical diffraction limit. For instance, scanning tunneling microscopy has been used to probe the localized excitonic properties.[24,25] Scattering-type scanning near-field optical microscopy (s-SNOM) also demonstrates the capability to map excitonic responses[26,27] and exciton polaritons[28,29]

2311568 (1 of 7)

**ADVANCED
SCIENCE NEWS**

www.advancedsciencenews.com

**ADVANCED
MATERIALS**

www.advmat.de

Figure 1. General concept. a) Schematic showing transient s-SNOM to measure exciton dynamics in MoS$_2$. The pump and probe beams have a wavelength of 400 and 800 nm, respectively. b) The AFM tip can access the localized information of 2D MoS$_2$, such as the crystal interfaces and nanoscale strains.

in 2D TMDCs. The transient s-SNOM nanoimaging of exciton–polaritons further reveals their temporal evolution after femtosecond photoexcitation.[30–32] In addition, ultrafast terahertz s-SNOM has been established to probe the interlayer transport and phase transition of excitons in TMDCs with nanoscale inhomogeneity.[33,34]

2. Results and Discussion

Here, we report a transient s-SNOM in the visible-near-infrared spectral region[35] to measure nanoscale exciton dynamics in TMDCs. As illustrated in **Figure 1a**, an 800 nm probe beam and a 400 nm pump beam with a controlled time delay (Δt) are directed onto an atomic force microscope (AFM) tip (see Experimental Section for more details on the experimental setup). The local excitonic properties can be probed via strong near-field interactions between the tip apex and the sample. Our probe beam is close to the excitonic transition energies of TMDCs, which is sensitive to the change of local dielectric function induced by photoexcited excitons. Thus, information on exciton dynamics can be obtained by analyzing the transient evolution of the scattered probe beam. The AFM tip enables a sub-50 nm spatial resolution to characterize the effects of nanoscale heterogeneities, such as crystal interfaces and localized strains (Figure 1b), on the excitonic responses. With the high spatiotemporal resolution and easy implementation, the transient near-field nanoscopy brings additional advantages compared to other tools for advancing TMDC research and accelerating their practical applications (Figure S1, Supporting Information).

We measure few-layer MoS$_2$ flakes prepared by mechanical exfoliation (**Figure 2a**). The monolayer and bilayer regions can be distinguished from optical images and confirmed by PL and Raman spectroscopy (Figure 2b; Figure S2, Supporting Information). The layer number is further characterized by probe-only static s-SNOM imaging. The amplitude image shows nearly uniform responses from the substrate, monolayer, and bilayer regions with clear boundaries (Figure S3, Supporting Information). To probe the spatiotemporal behavior of excitons in MoS$_2$ flakes, we scan the sample underneath the AFM tip to acquire the transient s-SNOM images at each time delay (Figure 2c). These images reveal evident dynamics with nanoscale heterogeneity where monolayer and bilayer MoS$_2$ yield distinct responses. To better present the departures, we plot the evolution of the near-field amplitude along a line traversing the sample (white dashed line in

Figure 2c). Such a spatiotemporal map captures the nanoscale dynamics of the sample (Figure 2d). Notably, the s-SNOM amplitude in the bilayer region drops significantly within ≈20 ps, while the monolayer MoS$_2$ shows a much slower decay. This variation can also be clearly visualized from the averaged transient s-SNOM amplitude profiles in Figure 2e. We further demonstrate the nanoscale resolution of transient s-SNOM to reveal exciton behaviors near the monolayer-bilayer interface, where the exciton dynamics differ from the faraway counterparts (Figure S4, Supporting Information).

To understand the transient s-SNOM data of MoS$_2$, we adopt the point-dipole model to interpret our observations (**Figure 3a**, Section S5, Supporting Information).[36] The point-dipole model can effectively capture the response of atomically thin layers on thick substrates.[26] The time-resolved s-SNOM profiles can be analyzed by the dynamic change of the dielectric function ε of MoS$_2$:[30]

$$\varepsilon(\omega, \Delta t) = \varepsilon_{stat}(\omega) + \Delta\varepsilon(\omega, \Delta t) \tag{1}$$

where ω and Δt are the photon energy and time delay, respectively. ε_{stat} is the equilibrium dielectric function that can be described by the Lorentz model (Figure S5, Supporting Information),[37] and $\Delta\varepsilon$ accounts for the change in dielectric function caused by pump beam illumination, which is a function of photoexcited exciton density $N(\Delta t)$ (Section S7, Supporting Information).[30,31] Therefore, by feeding Equation (1) to the point-dipole model, we can calculate the s-SNOM amplitude as a function of the exciton density (Figure 3c). For both monolayer and bilayer MoS$_2$, the calculated s-SNOM amplitude rises dramatically at the exciton density $N \approx 10^{18}$–10^{19} cm^{-3}.
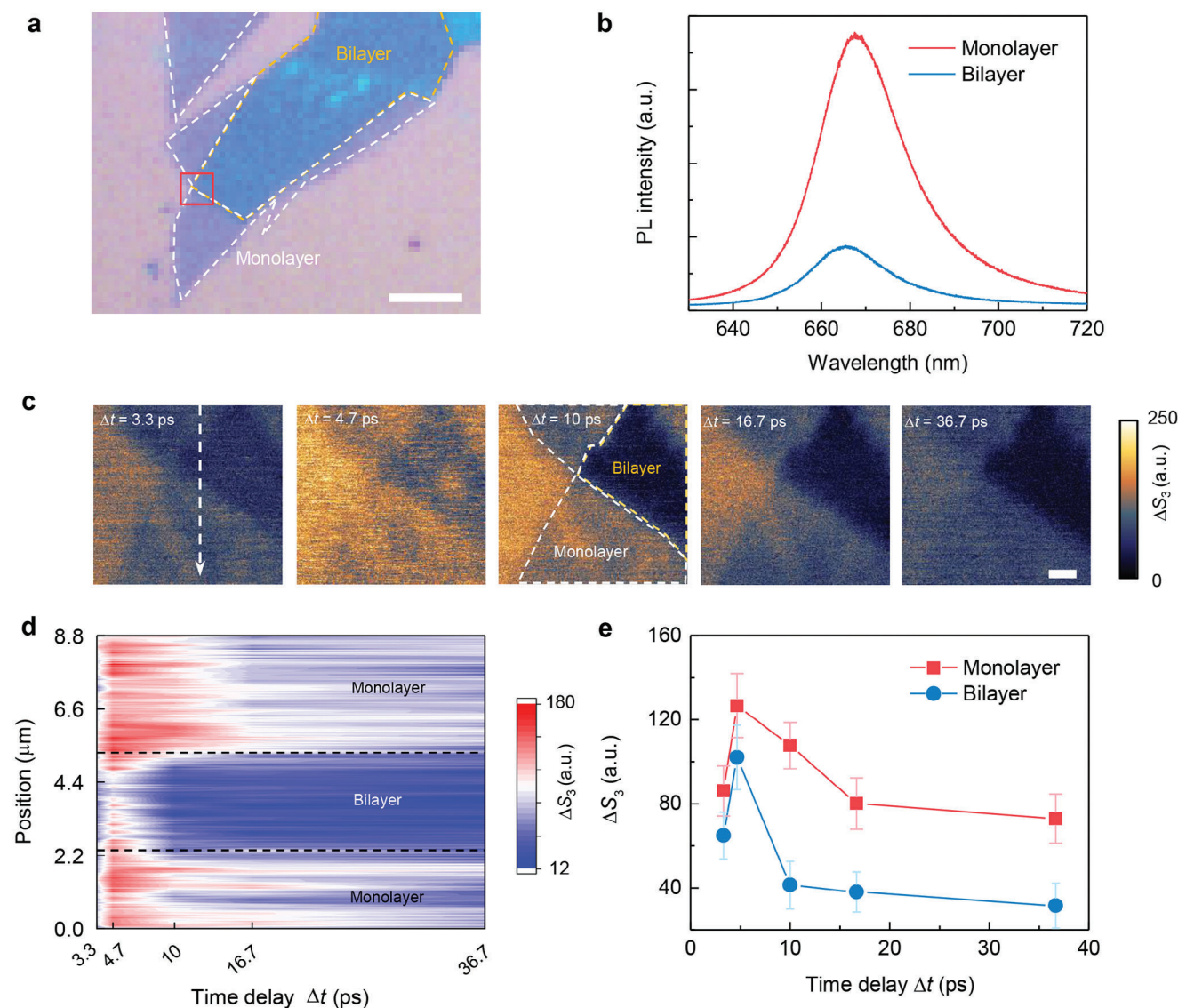
The exciton dynamics of MoS$_2$ can be described with a decay and an EEA (Figure 3b):[16]

$$\frac{dN}{d\Delta t} = -\frac{N}{\tau} - kN^2 \tag{2}$$

with the solution

$$N(\Delta t) = \frac{N(0)\exp\left(-\frac{\Delta t}{\tau}\right)}{1 + k\tau N(0)\left[1 - \exp\left(-\frac{\Delta t}{\tau}\right)\right]} \tag{3}$$

$N(\Delta t)$ is the exciton density at a delay time Δt, τ is the exciton lifetime without annihilation, and k is the EEA rate. By

ADVANCED
SCIENCE NEWS

www.advancedsciencenews.com

**ADVANCED
MATERIALS**

www.advmat.de

Figure 2. Transient s-SNOM measurement of monolayer and bilayer MoS$_2$. a) Optical image of the exfoliated MoS$_2$ flake. b) PL spectra of monolayer and bilayer MoS$_2$. c) Transient s-SNOM imaging of the rectangle region in (a) with delay time Δt = 3.3, 4.7, 10, 16.7, and 36.7 ps. d) Spatiotemporal map of the near-field amplitude along the dashed arrow line in (c). e) The averaged transient s-SNOM profiles on monolayer and bilayer MoS$_2$ extracted from (d). Scale bars: a) 10 μm; c) 1 μm.

integrating Equations (1)–(3) with Figure 3c, we can calculate the transient s-SNOM responses related to the exciton dynamics.

The transient s-SNOM profiles of monolayer and bilayer MoS$_2$ with a better temporal resolution are presented in Figure 3d,e, where our calculations (dashed curves) agree very well with the data (connected dots). We extract the exciton lifetime of monolayer and bilayer MoS$_2$ to be 449.4 and 9.1 ps, respectively. The radiative recombination of monolayer MoS$_2$ is usually faster than that of the bilayer,[38] and this experimental lifetime is dominated by the nonradiative processes.[14] The observed much shorter lifetime in bilayer MoS$_2$ is likely related to the enhanced exciton–phonon scattering.[39] Notably, the EEA rates of monolayer and bilayer MoS$_2$ are determined as 0.06 and 0.03 cm^2 s^{-1}, respectively. The larger EEA rate of monolayer MoS$_2$ is ascribed to stronger many-body interactions and direct bandgap at the mono-

layer limit (Figure S6, Supporting Information).[15,16] We also measure the dynamics under different exciton densities by tuning the pump beam intensity (Figure 3f). The results show that the bimolecular EEA process depends on the exciton density,[40] and the EEA rate decreases with the reduced pump power (Figure S7, Supporting Information).

In addition to the difference in monolayer and bilayer, the excitonic properties of TMDCs can also be affected by various physical and chemical facts, including defects, dopants, and strains.[22,41,42] Here, we study the strain effects from naturally formed wrinkles in exfoliated monolayer MoS$_2$ (**Figure 4a**; Figure S8, Supporting Information). The nano-wrinkle has a size of less than 100 nm, which is challenging to access by far-field optical techniques. By scanning the sample underneath the tip, we acquire the time-resolved near-field imaging of the nano-wrinkle to
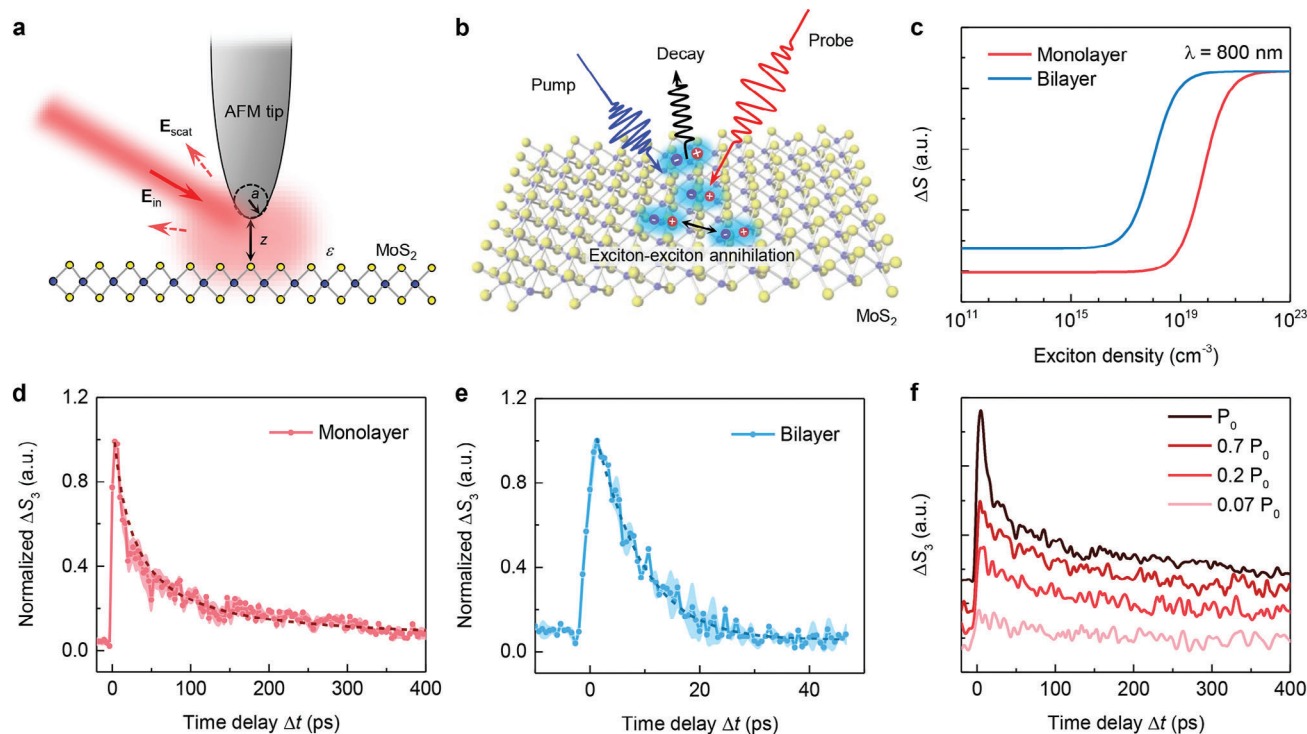
Figure 3. Transient s-SNOM data on exciton dynamics. a) Schematic of the point-dipole model. E_{in} and E_{scat} are the incident and scattered light, respectively. a, z, and ε are the AFM tip radius, tip-sample distance, and sample permittivity, respectively. b) Schematic showing the exciton relaxation pathways in MoS_2. c) Calculated s-SNOM amplitude for monolayer and bilayer MoS_2 as a function of exciton density. d,e) Experimental transient s-SNOM data (dots) and fitting curves (dashed line) of d) monolayer and e) bilayer MoS_2. The shading area indicates standard errors from multiple measurements. f) Transient s-SNOM scans of monolayer MoS_2 measured under different pump intensities.

reveal the spatially-resolved exciton dynamics. Before the pump beam arrives (Δt_1), the near-field amplitude is lower at the nano-wrinkle (Figure 4b), which is due to the existence of an air void that leads to a smaller effective refractive index (Section S11, Supporting Information).[43] After the photoexcitation, the nano-wrinkle becomes brighter in the near-field image (Figure 4c), which is ascribed to a higher exciton density due to the exciton funneling effect (Figure S10, Supporting Information).[21,44,45] This contrast in near-field amplitude persists at longer time delays (Figure 4d). The trend is consistent with the transient s-SNOM profiles measured at the flat flake and the MoS_2 nano-wrinkle (Figure 4e). The transient s-SNOM measurement also unambiguously reveals the difference in exciton dynamics between the flat and wrinkled regions (Figure 4f). Notably, the EEA rate of the nano-wrinkle is reduced by more than 40% compared with the flat flake.

This EEA suppression observed at the nanowrinkles is due to the strain-induced exciton transition energy shift. In general, the EEA process involves two excitons, and the final state consists of a high-energy electron and hole with an energy difference of $2E_X$, where E_X is the exciton transition energy. The presence of strain can shift the exciton transition energy E_X, after which the density of possible final states at $2E_X$ is reduced to suppress EEA.[17] On this account, unlike the flat monolayer, the EEA rate at the strained wrinkle is independent of the pump intensity (Figure S11, Supporting Information).[46] Besides MoS_2, we further demonstrate the general applicability of our transient
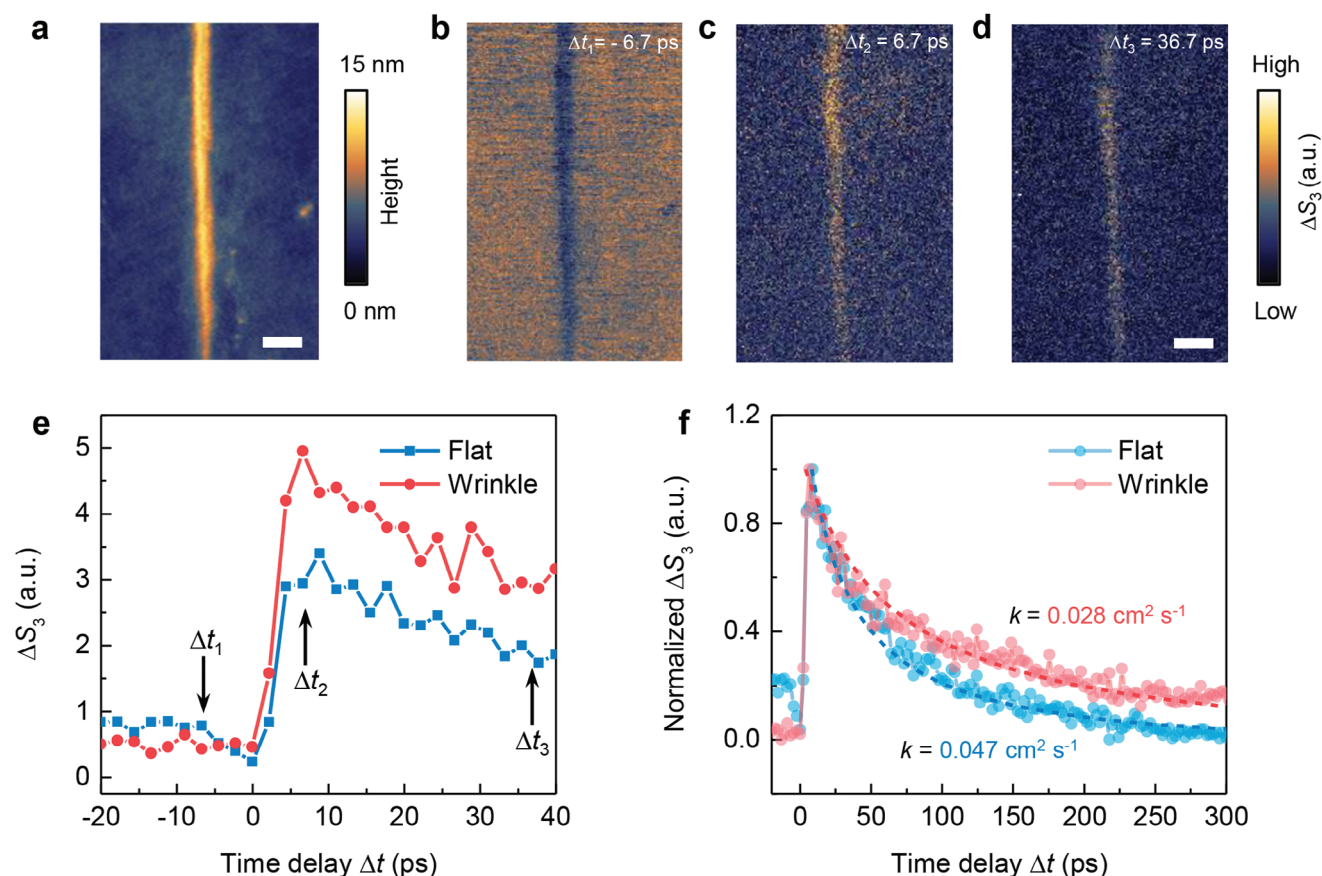
nanoscopy to probe nanoscale exciton dynamics in other TMDCs, such as $MoSe_2$ (Figure S12, Supporting Information).

3. Conclusions

In summary, we have studied the nanoscale exciton dynamics in atomically thin TMDCs using transient near-field nanoscopy. In addition to establishing the physical framework to understand the time-resolved near-field responses, we demonstrate the capability to probe local straining effects on excitonic properties. With high spatial resolution beyond the diffraction limit, our tip-based nanoscopy opens new possibilities to unravel the roles of nanoscale heterogeneity on many intriguing physical properties of TMDC materials, such as strain-engineered exciton-to-trion conversion,[47,48] dark excitons,[49] and quantum light emission.[50] We further anticipate the applications of this tool to provide more insights on understanding the excitonic properties for future innovation of TMDC materials and devices.

4. Experimental Section

Materials and Characterizations: MoS_2 and $MoSe_2$ flakes were prepared by mechanical exfoliation from commercially available crystals (MoS_2 from SPI Supplies and $MoSe_2$ from HQ Graphene). PL and Raman spectra were obtained using a micro-PL and Raman measurement system (Renishaw) with an excitation laser wavelength of 532 nm.

**ADVANCED
SCIENCE NEWS**

www.advancedsciencenews.com

**ADVANCED
MATERIALS**

www.advmat.de

Figure 4. Probing strain effects on exciton dynamics at the nanoscale. a) AFM topography of a monolayer MoS$_2$ flake with nano-wrinkles. b-d) Transient s-SNOM imaging of the nano-wrinkle with a time delay of b) $\Delta t_1 = -6.7$ ps, c) $\Delta t_2 = 6.7$ ps, and d) $\Delta t_3 = 36.7$ ps. e) Transient s-SNOM curves measured at flat and wrinkled regions. f) Normalized transient s-SNOM data and fitting curves (dashed lines) of flat and wrinkled MoS$_2$. Scale bars: 200 nm.

Experimental Setup: The setup was developed based on a commercial scanning near-field optical microscopy system from Molecular Vista. The Pt-coated AFM tip had an apex radius of $\approx$25 nm and a tapping frequency Ω at $\approx$250 kHz. An 800 nm femtosecond laser beam (Spectra-Physics) was split by a beam splitter into a probe beam and a pump beam. The probe laser was p-polarized with a repetition rate of 80 MHz and a separation time of 12.5 ns between two adjacent pulses to avoid interference. The pump beam was frequency doubled by a beta barium borate crystal (Eksma Optics) and then amplitude-modulated by an acoustic–optic modulator. The modulation frequency was set to be the third harmonic of the tapping frequency of the AFM tip. The probe beam passed through a mechanical delay stage (Thorlabs) to control the delay time. Both beams were directed to the AFM tip with a parabolic mirror. The scattered probe beam was then collected by the parabolic mirror and redirected to an avalanche photodiode detector (Thorlabs) after it was interfered with a reference beam from the reference mirror, per the scheme known as homodyne detection. The signal from the avalanche photodiode detector (Thorlabs) was sent to a lock-in amplifier for signal demodulation at the same modulation frequency of the pump beam, that is, the third harmonic of the tapping frequency (ΔS_3), to suppress the background noise. A long-pass filter (Thorlabs) was placed before the detector to block the scattered pump beam.

Supporting Information

Supporting Information is available from the Wiley Online Library or from the author.

Conflict of Interest

The authors declare no conflict of interest.

Data Availability Statement

The data that support the findings of this study are available in the supplementary material of this article.

**ADVANCED
SCIENCE NEWS**

www.advancedsciencenews.com

**ADVANCED
MATERIALS**

www.advmat.de

[1] Q. H. Wang, K. Kalantar-Zadeh, A. Kis, J. N. Coleman, M. S. Strano, *Nat. Nanotechnol.* **2012**, *7*, 699.

[2] K. F. Mak, K. He, J. Shan, T. F. Heinz, *Nat. Nanotechnol.* **2012**, *7*, 494.

[3] S. Manzeli, D. Ovchinnikov, D. Pasquier, O. V. Yazyev, A. Kis, *Nat. Rev. Mater.* **2017**, *2*, 17033.

[4] G. Wang, A. Chernikov, M. M. Glazov, T. F. Heinz, X. Marie, T. Amand, B. Urbaszek, *Rev. Mod. Phys.* **2018**, *90*, 021001.

[5] K. He, N. Kumar, L. Zhao, Z. Wang, K. F. Mak, H. Zhao, J. Shan, *Phys. Rev. Lett.* **2014**, *113*, 026803.

[6] K. F. Mak, J. Shan, *Nat. Photonics* **2016**, *10*, 216.

[7] W. Choi, N. Choudhary, G. H. Han, J. Park, D. Akinwande, Y. H. Lee, *Mater. Today* **2017**, *20*, 116.

[8] D. Akinwande, C. Huyghebaert, C.-H. Wang, M. I. Serna, S. Goossens, L.-J. Li, H. S. P. Wong, F. H. L. Koppens, *Nature* **2019**, *573*, 507.

[9] B. Radisavljevic, A. Radenovic, J. Brivio, V. Giacometti, A. Kis, *Nat. Nanotechnol.* **2011**, *6*, 147.

[10] O. Lopez-Sanchez, D. Lembke, M. Kayci, A. Radenovic, A. Kis, *Nat. Nanotechnol.* **2013**, *8*, 497.

[11] S. Wu, S. Buckley, J. R. Schaibley, L. Feng, J. Yan, D. G. Mandrus, F. Hatami, W. Yao, J. Vučković, A. Majumdar, X. Xu, *Nature* **2015**, *520*, 69.

[12] D. A. Wheeler, J. Z. Zhang, *Adv. Mater.* **2013**, *25*, 2878.

[13] D.-H. Lien, S. Z. Uddin, M. Yeh, M. Amani, H. Kim, J. W. Ager, E. Yablonovitch, A. Javey, *Science* **2019**, *364*, 468.

[14] H. Shi, R. Yan, S. Bertolazzi, J. Brivio, B. Gao, A. Kis, D. Jena, H. G. Xing, L. Huang, *ACS Nano* **2013**, *7*, 1072.

[15] D. Sun, Y. Rao, G. A. Reider, G. Chen, Y. You, L. Brézin, A. R. Harutyunyan, T. F. Heinz, *Nano Lett.* **2014**, *14*, 5625.

[16] L. Yuan, L. Huang, *Nanoscale* **2015**, *7*, 7402.

[17] H. Kim, S. Z. Uddin, N. Higashitarumizu, E. Rabani, A. Javey, *Science* **2021**, *373*, 448.

[18] Q. Cui, F. Ceballos, N. Kumar, H. Zhao, *ACS Nano* **2014**, *8*, 2970.

[19] A. J. Goodman, D. H. Lien, G. H. Ahn, L. L. Spiegel, M. Amani, A. P. Willard, A. Javey, W. A. Tisdale, *J. Phys. Chem. C* **2020**, *124*, 12175.

[20] A. G. del Águila, Y. R. Wong, I. Wadgaonkar, A. Fieramosca, X. Liu, K. Vaklinova, S. Dal Forno, T. T. H. Do, H. Y. Wei, K. Watanabe, T. Taniguchi, K. S. Novoselov, M. Koperski, M. Battiato, Q. Xiong, *Nat. Nanotechnol.* **2023**, *18*, 1012.

[21] Y. Koo, Y. Kim, S. H. Choi, H. Lee, J. Choi, D. Y. Lee, M. Kang, H. S. Lee, K. K. Kim, G. Lee, K.-D. Park, *Adv. Mater.* **2021**, *33*, 2008234.

[22] Z. Luo, W. Zheng, N. Luo, B. Liu, B. Zheng, X. Yang, D. Liang, J. Qu, H. Liu, Y. Chen, Y. Jiang, S. Chen, X. Zou, A. Pan, *Nano Lett.* **2022**, *22*, 2112.

[23] A. Sood, J. B. Haber, J. Carlström, E. A. Peterson, E. Barre, J. D. Georgaras, A. H. M. Reid, X. Shen, M. E. Zajac, E. C. Regan, J. Yang, T. Taniguchi, K. Watanabe, F. Wang, X. Wang, J. B. Neaton, T. F. Heinz, A. M. Lindenberg, F. H. da Jornada, A. Raja, *Nat. Nanotechnol.* **2023**, *18*, 29.

[24] S. Shabani, T. P. Darlington, C. Gordon, W. Wu, E. Yanev, J. Hone, X. Zhu, C. E. Dreyer, P. J. Schuck, A. N. Pasupathy, *Nano Lett.* **2022**, *22*, 7401.

[25] D. Huang, J. Choi, C.-K. Shih, X. Li, *Nat. Nanotechnol.* **2022**, *17*, 227.

[26] S. Zhang, B. Li, X. Chen, F. L. Ruta, Y. Shao, A. J. Sternbach, A. S. McLeod, Z. Sun, L. Xiong, S. L. Moore, X. Xu, W. Wu, S. Shabani, L.

[27] Zhou, Z. Wang, F. Mooshammer, E. Ray, N. Wilson, P. J. Schuck, C. R. Dean, A. N. Pasupathy, M. Lipson, X. Xu, X. Zhu, A. J. Millis, M. Liu, J. C. Hone, D. N. Basov, *Nat. Commun.* **2022**, *13*, 542.

[27] R. Jing, Y. Shao, Z. Fei, C. F. B. Lo, R. A. Vitalone, F. L. Ruta, J. Staunton, W. J. C. Zheng, A. S. McLeod, Z. Sun, B.-y. Jiang, X. Chen, M. M. Fogler, A. J. Millis, M. Liu, D. H. Cobden, X. Xu, D. N. Basov, *Nat. Commun.* **2021**, *12*, 5594.

[28] F. Hu, Y. Luan, M. E. Scott, J. Yan, D. G. Mandrus, X. Xu, Z. Fei, *Nat. Photonics* **2017**, *11*, 356.

[29] D. Hu, X. Yang, C. Li, R. Liu, Z. Yao, H. Hu, S. N. G. Corder, J. Chen, Z. Sun, M. Liu, Q. Dai, *Nat. Commun.* **2017**, *8*, 1471.

[30] A. J. Sternbach, S. Latini, S. Chae, H. Hübener, U. De Giovannini, Y. Shao, L. Xiong, Z. Sun, N. Shi, P. Kissin, G.-X. Ni, D. Rhodes, B. Kim, N. Yu, A. J. Millis, M. M. Fogler, P. J. Schuck, M. Lipson, X. Y. Zhu, J. Hone, R. D. Averitt, A. Rubio, D. N. Basov, *Nat. Commun.* **2020**, *11*, 3567.

[31] A. J. Sternbach, S. H. Chae, S. Latini, A. A. Rikhter, Y. Shao, B. Li, D. Rhodes, B. Kim, P. J. Schuck, X. Xu, X.-Y. Zhu, R. D. Averitt, J. Hone, M. M. Fogler, A. Rubio, D. N. Basov, *Science* **2021**, *371*, 617.

[32] M. Mrejen, L. Yadgarov, A. Levanon, H. Suchowski, *Sci. Adv.* **2019**, *5*, eaat9618.

[33] T. Siday, F. Sandner, S. Brem, M. Zizlsperger, R. Perea-Causin, F. Schiegl, S. Nerreter, M. Plankl, P. Merkl, F. Mooshammer, M. A. Huber, E. Malic, R. Huber, *Nano Lett.* **2022**, *22*, 2561.

[34] M. Plankl, P. E. Faria Junior, F. Mooshammer, T. Siday, M. Zizlsperger, F. Sandner, F. Schiegl, S. Maier, M. A. Huber, M. Gmitra, J. Fabian, J. L. Boland, T. L. Cocker, R. Huber, *Nat. Photonics* **2021**, *15*, 594.

[35] J. Li, R. Yang, Y. Rho, P. Ci, M. Eliceiri, H. K. Park, J. Wu, C. P. Grigoropoulos, *Nano Lett.* **2023**, *23*, 1445.

[36] Z. Fei, G. O. Andreev, W. Bao, L. M. Zhang, A. S. McLeod, C. Wang, M. K. Stewart, Z. Zhao, G. Dominguez, M. Thiemens, M. M. Fogler, M. J. Tauber, A. H. Castro-Neto, C. N. Lau, F. Keilmann, D. N. Basov, *Nano Lett.* **2011**, *11*, 4701.

[37] Y. Li, A. Chernikov, X. Zhang, A. Rigosi, H. M. Hill, A. M. van der Zande, D. A. Chenet, E.-M. Shih, J. Hone, T. F. Heinz, *Phys. Rev. B* **2014**, *90*, 205422.

[38] M. Palummo, M. Bernardi, J. C. Grossman, *Nano Lett.* **2015**, *15*, 2794.

[39] A. Raja, M. Selig, G. Berghäuser, J. Yu, H. M. Hill, A. F. Rigosi, L. E. Brus, A. Knorr, T. F. Heinz, E. Malic, A. Chernikov, *Nano Lett.* **2018**, *18*, 6135.

[40] L. Yuan, J. Jeong, K. W. Chi Kwock, E. S. Yanev, M. Grandel, D. A. Rhodes, T. S. Luk, P. J. Schuck, D. Yarotski, J. C. Hone, I. Brener, R. P. Prasankumar, *Nano Lett.* **2021**, *21*, 9930.

[41] G.-Y. Huang, L. Lin, S. Zhao, W. Li, X. Deng, S. Zhang, C. Wang, X.-Z. Li, Y. Zhang, H.-H. Fang, Y. Zou, P. Li, B. Bai, H.-B. Sun, T. Fu, *Nano Lett.* **2023**, *23*, 1514.

[42] I. Niehues, R. Schmidt, M. Drüppel, P. Marauhn, D. Christiansen, M. Selig, G. Berghäuser, D. Wigger, R. Schneider, L. Braasch, R. Koch, A. Castellanos-Gomez, T. Kuhn, A. Knorr, E. Malic, M. Rohlfing, S. Michaelis de Vasconcellos, R. Bratschitsch, *Nano Lett.* **2018**, *18*, 1751.

[43] R. Yang, J. Li, C. P. Grigoropoulos, *J. Phys. Chem. C* **2024**, *128*, 261.

[44] A. Castellanos-Gomez, R. Roldán, E. Cappelluti, M. Buscema, F. Guinea, H. S. J. van der Zant, G. A. Steele, *Nano Lett.* **2013**, *13*, 5361.

[45] H. Lee, Y. Koo, J. Choi, S. Kumar, H.-T. Lee, G. Ji, S. H. Choi, M. Kang, K. K. Kim, H.-R. Park, H. Choo, K.-D. Park, *Sci. Adv.* **2022**, *8*, eabm5236.

[46] S. Z. Uddin, N. Higashitarumizu, H. Kim, J. Yi, X. Zhang, D. Chrzan, A. Javey, *ACS Nano* **2022**, *16*, 8005.

[47] H. Lee, Y. Koo, S. Kumar, Y. Jeong, D. G. Heo, S. H. Choi, H. Joo, M. Kang, R. H. Siddique, K. K. Kim, H. S. Lee, S. An, H. Choo, K.-D. Park, *Nat. Commun.* **2023**, *14*, 1891.

2311568 (6 of 7)

[48] Y. Koo, H. Lee, T. Ivanova, A. Kefayati, V. Perebeinos, E. Khestanova, V. Kravtsov, K.-D. Park, *Light: Sci. Appl.* **2023**, *12*, 59.

[49] R. Sebait, R. Rosati, S. J. Yun, K. P. Dhakal, S. Brem, C. Biswas, A. Puretzky, E. Malic, Y. H. Lee, *Nat. Commun.* **2023**, *14*, 5548.

[50] X. Li, A. C. Jones, J. Choi, H. Zhao, V. Chandrasekaran, M. T. Pettes, A. Piryatinski, M. A. Tschudin, P. Reiser, D. A. Broadway, P. Maletinsky, N. Sinitsyn, S. A. Crooker, H. Htoon, *Nat. Mater.* **2023**, *22*, 1311.

2311568 (7 of 7)